physica status solidi a
www.pss-a.com

Check for updates

Effect of GaN/AlGaN Buffer Thickness on the Electrothermal Performance of AlGaN/GaN High Electron Mobility Transistors on Engineered Substrates

Marko J. Tadjer, Patrick Waltereit, Lutz Kirste, Stefan Müller, James Spencer Lundh, Alan G. Jacobs, Andrew D. Koehler, Pavel Komarov, Peter Raad, John Gaskins, Patrick Hopkins, Vlad Odnoblyudov, Cem Basceri, Travis J. Anderson, and Karl D. Hobart*

AlGaN/GaN high electron mobility transistors on QST engineered substrates are grown with different GaN/AlGaN buffer layer thickness. The as-grown heterostructures are evaluated for their structural quality via atomic force microscopy, high-resolution X-ray diffraction, Raman spectroscopy, and steady-state thermoreflectance. Transistor devices are fabricated and evaluated via DC and pulsed electrical techniques, as well as thermoreflectance imaging. It is reported that buffer layer thickness of at least 10 μm can result in lateral high electron mobility transistors (HEMTs) with simultaneously high GaN quality, low stress, good DC electrical performance, low current collapse, and low thermal resistance.

1. Introduction

AlGaN/GaN high electron mobility transistors (HEMTs) are an important class of commercial power and radio frequency devices with applications in the communications, data center, and defense markets, among others. Although GaN HEMTs have been demonstrated on a variety of substrates, commercially available devices are grown heteroepitaxially on Si or SiC substrates. The development of III-Nitride HEMTs on large-area, low-cost engineered substrates leverages the ability to closely match the coefficient of thermal expansion (CTE) of a polycrystalline AlN substrate core to that of GaN to within a percent (**Table 1**).[1] By comparison, the CTE mismatch of GaN with Si and 4H-SiC is 54% and 25%, respectively, although GaN and 4H-SiC are closely matched in terms of lattice parameter (3.5% mismatch). As a result, the use of cost-effective engineered substrates, commercialized by Qromis, results in low bow, crack-free, thick GaN/AlGaN buffer layers over the largest diameter (200 mm) substrates possible for GaN epitaxy.[2–10] We have previously demonstrated improved drain current, breakdown voltage, and reduced peak device temperature by doubling the total buffer layer thickness from 3 μm on GaN-on-Si to 6 μm using GaN-on-QST technology.[5] The improved HEMT thermal performance reported in ref. [5] suggested that the superior thermal conductivity of AlN could have further contributed; however, a detailed study comparing electrothermal performance of GaN-on-QST HEMTs with different buffer layer thicknesses has not been performed to date. This work further quantifies the effect of increasing GaN buffer thickness in GaN-on-QST wafers using up to 15 μm-thick GaN/AlGaN buffer layers and comparing their structural, electrical (DC and pulsed), and thermal performance.

M. J. Tadjer, A. G. Jacobs, A. D. Koehler, T. J. Anderson, K. D. Hobart
Electronics Science and Technology Division
United States Naval Research Laboratory
Washington, DC 20375, USA
E-mail: marko.tadjer@nrl.navy.mil

P. Waltereit, L. Kirste, S. Müller
Fraunhofer Institute for Applied Solid State Physics
79108 Freiburg, Germany

J. S. Lundh
National Research Council Postdoctoral Fellow
Residing at NRL
Washington, DC 20375, USA

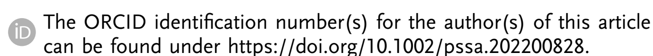
The ORCID identification number(s) for the author(s) of this article can be found under https://doi.org/10.1002/pssa.202200828.

DOI: 10.1002/pssa.202200828

P. Komarov, P. Raad
TMX Scientific
Richardson, TX 75081, USA

P. Raad
Department of Mechanical Engineering
Southern Methodist University
Dallas, TX 75205, USA

J. Gaskins, P. Hopkins
LaserThermal Inc.
Charlottesville, VA 22902, USA

P. Hopkins
Mechanical and Aerospace Engineering
University of Virginia
Charlottesville, VA 22904, USA

V. Odnoblyudov, C. Basceri
Qromis Inc.
San Francisco, CA 95051, USA

© 2023 Wiley-VCH GmbH

Table 1. Comparison of substrates for GaN epitaxy based on lattice and thermal mismatch.[1] Lattice parameter, thermal conductivity, relative cost, and diameter are shown for each substrate material.

Substrate	a [Å]	Thermal cond., κ [W cm^{-1} K^{-1}]	In-plane CTE @ 700 K [ppm K^{-1}]	Lattice mismatch GaN/sub [%]	Thermal mismatch GaN/sub [%]	Max substrate diameter with GaN Epi [mm]	Cost
GaN	3.184	1.3	5.59	0	0	100	$$$
AlN	3.110	4.2	5.55	2.4	≈1	50	$$$$$
Si(111)	5.430	1.4	2.59	−16.9	54	300	$
4H-SiC	3.073	3.8	4.44	3.5	25	200	$$
Sapphire	4.758	0.5	7.50	16	−34	200	$$
QST	5.430	1.8–2.0	5.41	−16.9	≈1	200	$

Table 2. Comparison of AlGaN/GaN HEMT specifications in the present study.

Sample	SiN cap [nm]	GaN cap [nm]	AlN [nm]	AlGaN [nm]	Al ratio [%]	UID GaN [nm]	T_{BUFFER} (GaN/AlGaN) [μm]
A	3	1	2	N/A	100	150	3
B	0	2	N/A	16	22	150	5
C	0	1	N/A	16	25	500	10
D	0	2	N/A	20	20	150	15
Ref.	0	0	N/A	≈20	≈20	≈1.5 μm total T_{BUFFER}	

Table 3. Sheet resistance, Hall mobility, and carrier concentration measured for the samples at room temperature using the Hall technique.

Sample	R_{SH} [Ω sq.$^{-1}$]	μ_{HALL} [cm^2 V^{-1} s^{-1}]	N_{SH} [×10^{12} cm^{-2}]
A	N/A	N/A	N/A
B	635	1116	8.81
C	503	1357	9.15
D	534	1492	7.84
Ref.	592–503	1892–1938	5.5–6.4

2. Experimental Section

AlGaN/GaN heterostructures were grown by metal organic chemical vapor deposition (MOCVD) on QST substrates, which consisted of a polycrystalline AlN core and a number of engineered layers, the final of which was (111) Si which provided a nucleation surface for nucleation of the MOCVD III-Nitride layers. Four samples were grown and processed using standard microfabrication techniques (Cl-plasma ICP mesa etch, Ti/Al/Ni/Au Ohmic contacts alloyed by rapid-thermal annealing at 850 °C for 30 s in N_2, Ni/Au gate lift-off, 100 nm-thick PECVD SiN passivation). Details of sample structures are shown in **Table 2**, where T_{BUFFER} refers to the total thickness of the GaN/AlGaN buffer layers underneath an unintentionally doped (UID) GaN layer. Sample A had a 3 nm SiN cap and an AlN barrier layer. On this sample, the SiN cap was exposed to SF_6 plasma etch for 90 s immediately prior to Ohmic contact deposition. While the etch rate for in situ MOCVD-grown SiN was not calibrated, it is significantly lower than that of PECVD SiN (≈100 nm min^{-1}). Nevertheless, a high contact resistance was measured on this sample, suggesting that the SiN cap may not have been completely etched off. Samples B–D were nominally similar: 1–2 nm GaN cap and 16–20 nm-thick AlGaN barrier with 20–25% Al ratio. The reference commercial AlGaN/GaN HEMT on Si substrate had approximately 20 nm-thick AlGaN barrier layer with about 20% Al ratio, and a 1.5 μm-thick GaN buffer layer. Hall measurements were performed on all five samples and are summarized in **Table 3**. Sample A exhibited higher contact resistance which prevented measurement of Hall characteristics in our Lakeshore M91 FastHall system. Device geometries were $L_G = 3$ μm, $W = 75$ μm, $L_{GS} = 2.5$ μm, and $L_{GD} = 10$ μm.

Atomic force microscopy (AFM) and high-resolution X-ray diffraction (HRXRD) were performed using a Bruker Dimension ICON AFM and a Panalytical MRD, Cu Kα_1 radiation, Ge 2 × 220 monochromator, and triple axis Ge 220 analyzer. Raman spectra from the four samples were obtained using a polarized 532 nm wavelength excitation laser source and 100× objective in a 180° backscattering configuration. The power of the laser was limited to 5 mW to prevent laser heating of the engineered layers in the QST substrate. DC I–V measurements were performed using a Keithley 4200SCS semiconductor parameter analyzer. Dynamic on-resistance was extracted from pulsed-mode I–V measurements performed using a DiVA pulsed measurement instrument. Thermal conductivity measurements of the as-grown epitaxial layers were performed using a LaserThermal SSTR-F steady-state thermoreflectance (SSTR) measurement system. Device-level TR characterization was performed on a TMX Scientific T°Imager transient TR imaging system with a 100× near-UV objective at 365 nm illumination wavelength. The measured change in reflectance ($\Delta R/R$) is proportional to the change in temperature as described by the TR relationship

$$\Delta T = (\Delta R/R)/\mathrm{CTR} \quad (1)$$

where CTR is the pixel-by-pixel calibrated coefficient of TR. The accuracy of the TR imaging technique was within 1 °C for over 95% of the pixels. Details of the TR methods have been published elsewhere in the literature.[11–13]

© 2023 Wiley-VCH GmbH

18626319, 2023, 16, Downloaded from https://onlinelibrary.wiley.com/doi/10.1002/pssa.202200828 by University Of Virginia Claude Moore, Wiley Online Library on [10/02/2024]. See the Terms and Conditions (https://onlinelibrary.wiley.com/terms-and-conditions) on Wiley Online Library for rules of use; OA articles are governed by the applicable Creative Commons License

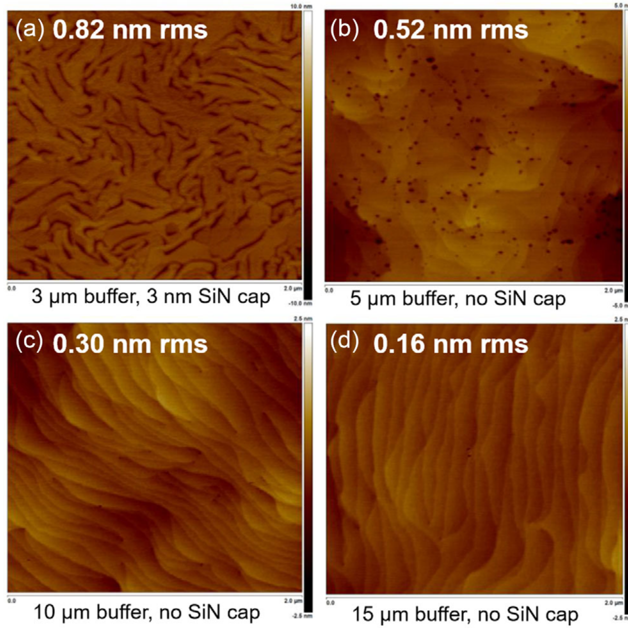

Figure 1. AFM images of the epitaxial surface of samples A–D. Note the 3 nm-thick SiN cap on sample A, which also had AlN barrier layer. Root mean square (rms) roughness for each sample is inversely proportional to buffer thickness.

3. Results and Discussion

Figure 1 shows the $2 \times 2\,\mu m$ AFM scans of samples A–D. Sample A (Figure 1a) resulted in the highest root mean square (rms) roughness of all four samples, 0.82 nm, which could have been due to partial relaxation of the AlN barrier layer as well as the higher stress in the GaN layers, as measured by Raman spectroscopy (see **Table 4**). Sample B presented a large density of threading dislocations in the AFM image (Figure 1b) which also resulted in higher roughness (0.52 nm rms) compared to samples C and D (0.30 and 0.16 nm, respectively). Overall, the surface roughness decreased as the GaN/AlGaN buffer became thicker, likely as a result of improved epilayer quality and reduced stress in the GaN layers, as measured by HRXRD and Raman spectroscopy. In **Figure 2**, HRXRD scans of the four samples showing the 0002 GaN reflection were obtained. The HRXRD omega scans for the 0002 and −1102 GaN reflections are presented in **Figure 3**. At full width at half maximum (FWHM), the width of each measured omega scan reflection for samples A–D is also summarized in Table 4. While comparable for samples A and B, FWHM values show a decreasing trend as the buffer thickness is increased from 5 to 15 μm (samples B–D). The full-width at half maxima decrease as the buffer layers become thicker, showing improved quality of GaN. We attribute this effect to the improved CTE match with the engineered substrate. In the case of HEMTs grown on a Si substrate, an increasing 0002 reflection FWHM with increasing AlGaN back barrier thickness has been reported, which is the opposite effect as the epilayer will relax as it grows thicker.[14] The absence of threading dislocations in the AFM images for the 10 and 15 μm-thick buffer layers (Figure 1c,d) correlates well with the lower FWHM and stress values for these samples (Table 4).

In the Raman spectra of samples A–D (**Figure 4**), of note is the comparable intensity of the Si and GaN E_2 (high) peaks owing to the significantly thicker GaN layers as compared to commercial GaN-on-Si epiwafers. As shown in Figure 4a, as the thickness of the GaN layer increases from 3 to 15 μm, the GaN E_2 (high) peak intensity increases $\approx 5\times$ while the Si peak intensity decreases $\approx 6\times$. For the 15 μm-thick GaN/AlGaN buffer, the E_2 (high) peak has an intensity $\approx 5\times$ greater than that of the Si peak; this is in stark contrast to typical Raman spectra of thickness-limited GaN films on Si, where the Si peak strongly dominates.[15]

In addition to the Raman peak intensity, the peak position and FWHM of the Raman peaks can also provide valuable insight regarding residual film stress and crystalline quality, respectively. These spectral features are indicative of the energy (peak position) and lifetime (FWHM) of the phonons at the Brillouin zone center.[16] For the $Z(XX)\bar{Z}$ Raman scattering geometry, the E_2 and A_1 (LO) modes are allowed[17] and can be seen in Figure 4b,c. The Raman spectra of the E_2 (high) and A_1 (LO) modes of the GaN layers show similar trends for samples A, B, and D (150 nm-thick UID GaN layer), namely, redshifting of the Raman peak position and a decrease in FWHM as the thickness of the GaN/AlGaN buffer layer increased (Table 4). The decrease in FWHM with increasing GaN/AlGaN buffer thickness for samples A, B, and D indicates that the crystalline quality of the GaN layers has improved because the likelihood of phonon scattering from grain boundaries, defects, and dislocations has decreased. Sample C did not follow the trend as it had a thicker UID GaN layer (500 nm, compared to 150 nm for samples A, B, and D). A redshift in the Raman peak position typically indicates that residual

Table 4. Comparison of the HRXRD FWHM of the 0002 and −1102 reflections in Figure 2 and the GaN A_1 (LO) phonon peak position and linewidth for samples A–D. A trend of improved crystallinity with increasing GaN/AlGaN buffer thickness was observed. The stress-free phonon frequencies of the GaN E_2 (high) and A_1 (LO) peaks are 568.15 ± 0.13 and $733.94 \pm 0.09\ cm^{-1}$, respectively.[19] The Raman biaxial stress coefficients of the GaN E_2 (high) and A_1 (LO) modes are -3.09 ± 0.41 and $-2.14 \pm 0.28\ cm^{-1}\ GPa^{-1}$, respectively. As with convention, a negative stress represents compressive stress.

Sample	$\Delta\omega$ 0002	$\Delta\omega$ −1102	GaN E_2 (high) position	GaN E_2 (high) width	Stress E_2 (high)	GaN A_1 (LO) position	GaN A_1 (LO) width	Stress A_1 (LO)
	[°]	[°]	[cm^{-1}]	[cm^{-1}]	[GPa]	[cm^{-1}]	[cm^{-1}]	[GPa]
A	0.2505	0.3670	570.429	8.779	−0.737.5	735.49	13.78	−0.7241
B	0.2669	0.3695	569.252	5.921	−0.3566	735.11	9.56	−0.5473
C	0.0920	0.2336	567.687	4.653	0.1499	734.11	7.46	−0.0804
D	0.0783	0.1885	568.026	5.0533	0.0400	734.36	7.54	−0.1970

© 2023 Wiley-VCH GmbH

18626319, 2023, 16, Downloaded from https://onlinelibrary.wiley.com/doi/10.1002/pssa.202200828 by University Of Virginia Claude Moore, Wiley Online Library on [10/02/2024]. See the Terms and Conditions (https://onlinelibrary.wiley.com/terms-and-conditions) on Wiley Online Library for rules of use; OA articles are governed by the applicable Creative Commons License

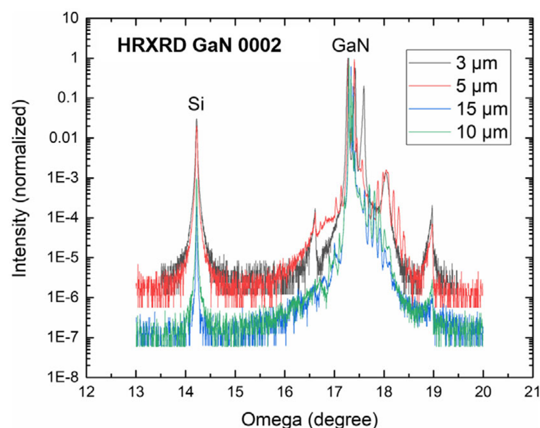

Figure 2. HRXRD scans of the GaN 0002 reflection on samples A–D.

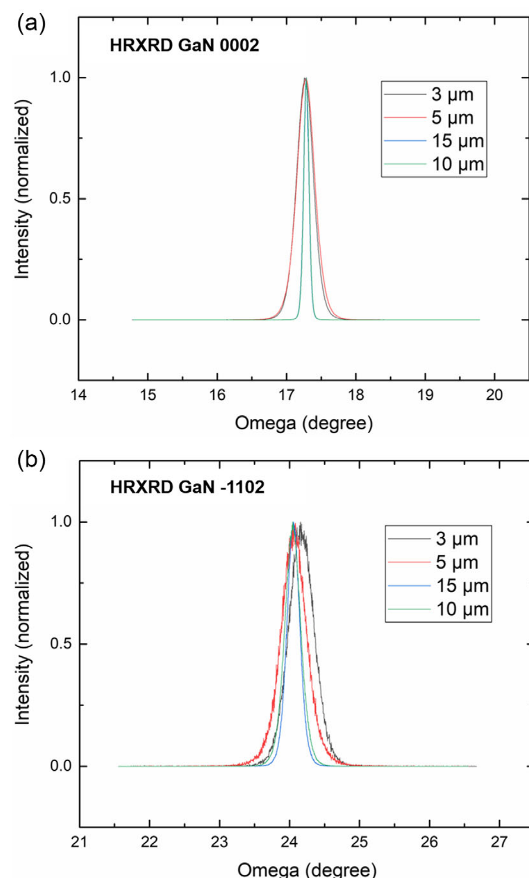

Figure 3. HRXRD omega scans on GaN/AlGaN buffers grown on QST substrates using the a) 0002 and b) −1102 GaN reflections.

film stress is becoming more tensile; however, if the stress-free phonon frequencies and Raman biaxial stress coefficients are known, Raman peak positions can be used to assess the type (compressive or tensile) and magnitude of residual stress. This relation is given by[18]

$$\omega_{\text{meas}} - \omega_0 = K^{\text{II}}\sigma_{xx} \tag{2}$$

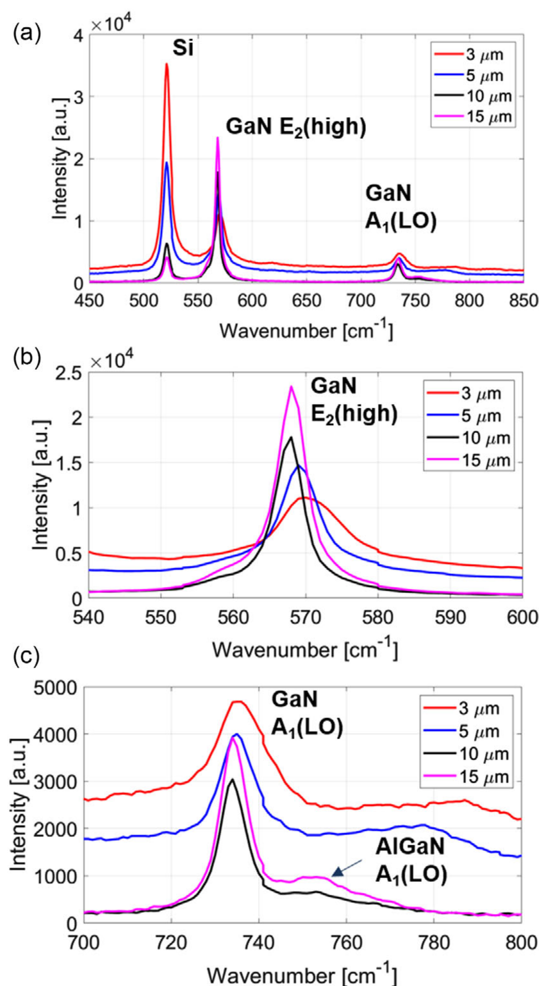

Figure 4. Raman spectra obtained from samples A–D using a 532 nm excitation wavelength.

where ω_{meas} is the measured phonon frequency (Raman peak position), ω_0 is the stress-free phonon frequency, K^{II} is the Raman biaxial stress coefficient, and σ_{xx} is the biaxial residual stress ($\sigma_{xx} = \sigma_{yy}$). For the GaN E_2 (high) and A_1 (LO) modes, the stress-free phonon frequencies and Raman biaxial stress coefficients have been reported previously by Choi et al.[19] Using these values for both phonon modes (see Table 4), the residual film stresses were determined for the GaN layers and are listed in Table 4. For the thinnest GaN/AlGaN buffer (3 μm), the film is measured to be compressively stressed with magnitudes of 738 and 724 MPa using the E_2 (high) and A_1 (LO) modes, respectively. Typical measurement uncertainties for stress calculations are 50–100 MPa. With increasing buffer thickness, the stress measured in the GaN film becomes less compressive and approaches a stress-free state.

Following materials characterization, HEMT structures were fabricated on the GaN films and electrical characterization was performed. DC I_{DS}–V_{GS} ($V_{\text{DS}} = 1$ V) and I_{DS}–V_{DS} current–voltage characteristics are presented in **Figure 5**. The AlN barrier of sample A resulted in more positive threshold voltage and lower on-state current at 1 V drain bias compared

© 2023 Wiley-VCH GmbH

18626319, 2023, 16, Downloaded from https://onlinelibrary.wiley.com/doi/10.1002/pssa.202200828 by University Of Virginia Claude Moore, Wiley Online Library on [10/02/2024]. See the Terms and Conditions (https://onlinelibrary.wiley.com/terms-and-conditions) on Wiley Online Library for rules of use; OA articles are governed by the applicable Creative Commons License

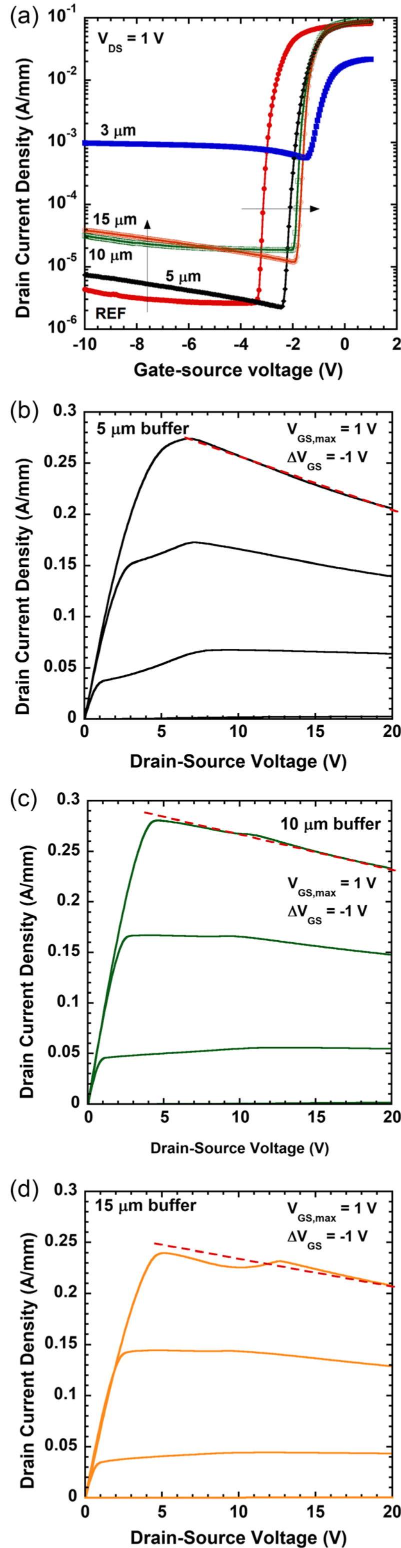

Figure 5. a) I_{DS}–V_{GS} characteristics for samples A–D with a GaN-on-Si reference sample. b–d) Representative I_{DS}–V_{DS} characteristics for the AlGaN/GaN HEMT with a 3–15 μm GaN/AlGaN buffer layers (samples B–D).

to the rest of the samples. In addition, sample A had much higher off-state leakage current, likely due to increase in plasma damage from the PECVD SiN passivation process, which was designed for the passivation of HEMTs with a thicker AlGaN barrier. Samples B–D and the reference AlGaN/GaN/Si HEMT exhibited a consistent trend in increasing off-state drain leakage current and turn-on voltage as the buffer thickness increased (Figure 5a). Prior literature has reported that higher compressive (more negative) stress in the buffer layer results in a negative shift in turn-on voltage.[20] The subthreshold slope also slightly improved, as shown in **Table 5**, suggesting that channel confinement was better with the thicker GaN/AlGaN buffer layer, which also acted as a back barrier. In the off-state, sample B (5 μm-thick GaN/AlGaN buffer) exhibited the lowest off-state drain current of all HEMTs on engineered substrate, similar to that of a control GaN-on-Si HEMT. Despite higher quality buffer layer demonstrated in the HRXRD data, samples C and D (10 and 15 μm-thick GaN/AlGaN buffer) exhibited about one of magnitude increase in $I_{DS,OFF}$ compared to sample B, likely due to increased buffer trap density. In the output characteristics (Figure 5b–d), measured from lower toward higher drain voltage, a noticeable kink in drain current in the on-state as the device transitions into the saturation region has been attributed to buffer traps due to carbon dopants by Cao et al.[21] The slope of the drain current in the saturation region ($I_{DS,SAT}$–V_{DS}, $V_{GS} = 0$ V) was used to compare differential output resistance ($\Delta V_{DS,SAT}/\Delta I_{DS,SAT}$) in samples B–D. Figure 5b–d shows a smaller change in drain current as the buffer layer was grown thicker, which suggested that self-heating effects were least severe for the HEMTs on sample D, which had the thickest GaN/AlGaN buffer layer.[22]

Current collapse via off-state quiescent drain voltage stress is one technique for quantifying the effect of trap states on HEMT performance.[23] The device is stressed in the off-state under quiescent conditions ($V_{GS,Q} = -6$ V, $V_{DS,Q} = 0$–50 V), followed by an on-resistance measurement in the on-state. Any increase in dynamic on-resistance $R_{ON,DYN}$ would be due to channel electrons trapping either near the surface or the buffer in the device. **Figure 6** shows that samples A and D, which had the thin AlN barrier layer and the thickest GaN/AlGaN buffer layers, respectively, had the highest change in $R_{ON,DYN}$. The degradation in $R_{ON,DYN}$ in sample A correlated well with the high DC off-state drain current $I_{DS,OFF}$ in that sample. On the other hand, the current collapse in sample D was more likely to have originated from traps in the 15 μm-thick GaN/AlGaN buffer layer, as that sample

Table 5. Comparison of relevant electrothermal parameters measured for samples A–D.

Sample	T_{BUFFER}	$I_{DS,OFF}$	V_{TH}	SS	R_{TH}
	(GaN/AlGaN) [μm]	$V_{GS} = -10$ V [A mm^{-1}]	[V]	[mV dec^{-1}]	[°C mm W^{-1}]
A	3	9.9×10^{-4}	−1.8 V	560	50.6
B	5	7.4×10^{-6}	−2.4 V	177	33.3
C	10	3.22×10^{-5}	−2.1 V	172	18.3
D	15	3.9×10^{-5}	−1.95 V	151	21

© 2023 Wiley-VCH GmbH

18626319, 2023, 16, Downloaded from https://onlinelibrary.wiley.com/doi/10.1002/pssa.202200828 by University Of Virginia Claude Moore, Wiley Online Library on [10/02/2024]. See the Terms and Conditions (https://onlinelibrary.wiley.com/terms-and-conditions) on Wiley Online Library for rules of use; OA articles are governed by the applicable Creative Commons License

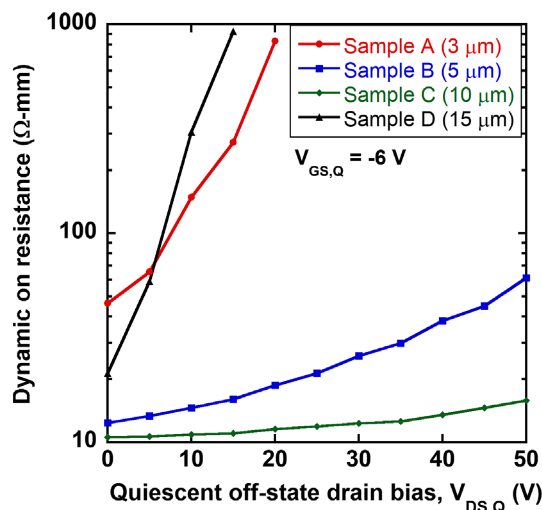

Figure 6. Pulsed-mode dynamic on-state resistance ($R_{ON,DYN}$) measurements as a function of quiescent drain bias $V_{DS,Q}$ for samples A–D using quiescent gate bias $V_{GS,Q} = -6$ V.

had $I_{DS,OFF}$ comparable to that of sample C. The fact that $R_{ON,DYN}$ in sample C changed from about 10 Ω mm at zero bias to about 15.9 Ω mm at $V_{DS,Q} = 50$ V supported our hypothesis that this sample exhibited optimal material and electrical properties.

We further support this hypothesis with TR measurements on as-grown epilayers and fabricated HEMT devices. **Figure 7** shows effective thermal conductivity k_{eff} of the as-grown samples A–D, measured via SSTR using a 4.15 and a 7.5 μm laser spot size. In the steady state, laser spot size correlates well with penetration depth into the film. For this reason, k_{eff} measurement on samples A and B using the 7.5 μm spot size likely included contributions from the QST substrate. Nevertheless, a linear trend of increasing k_{eff} with thicker GaN/AlGaN buffer was measureable in this sample set. The 500 nm-thick UID GaN layer in sample C (see Table 2) was the likely cause of measuring a higher k_{eff} of sample C compared to sample D (150 nm UID GaN).

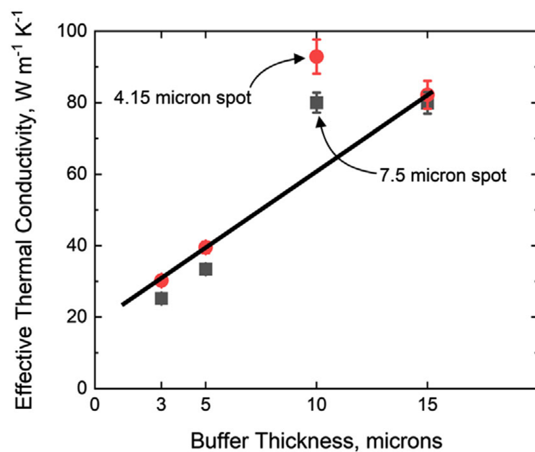

Figure 7. SSTR measurement of effective thermal conductivity across the as-grown epitaxial layers grown on QST substrates in samples A–D.

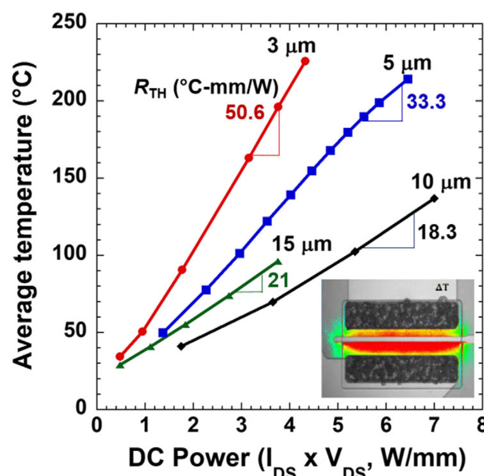

Figure 8. Average temperature as a function of DC power ($I_{DS} \times V_{DS}$) for samples A–D measured via TR imaging on fabricated HEMTs. Labeled curve slope indicates thermal resistance R_{TH} (°C mm W^{-1}). Also labeled on the figure is the total GaN/AlGaN buffer thickness for each HEMT sample. Inset: SSTR image of AlGaN/GaN HEMT.

Transient TR measurement of average temperature in the gate–drain region as a function of DC output power ($P_{OUT} = I_{DS} \times V_{DS}$) is presented in **Figure 8**. In the figure inset, a typical temperature distribution map obtained from the TR signal of the CTR-calibrated device according to Equation (1) is shown for reference. The average temperature in Figure 8 was obtained from averaging the temperature measurements across the gate–drain access regions minus an exclusion zone near the mesa edge. Device thermal resistance R_{TH} was obtained from the slope of the T_{AVG} versus P_{OUT} curve for each sample, showing good agreement with the k_{eff} measurements. We note that the slightly higher temperature for sample D (15 μm buffer) correlated well with the slightly lower k_{eff} measured via SSTR on that sample. The lowest thermal resistance was obtained from sample C, $R_{TH} = 18.3$ °C mm W^{-1}, as summarized in Table 5. While these R_{TH} values are comparable to thermal resistances reported for HEMTs on Si substrate, HEMTs on SiC and diamond substrates have been reported to exhibit much lower R_{TH} mainly due to the much thinner buffer layers in these heterostructures, as well as the high thermal conductivity of these substrates.[24,25]

4. Conclusion

AlGaN/GaN HEMTs were grown on Qromis QST engineered substrates using GaN/AlGaN buffer layers with thickness ranging from 3 to 15 μm, followed by growth of the device GaN/AlGaN regions with an undoped GaN layer in between. The effect of the buffer layer thickness was systematically evaluated first using material characterization (AFM, XRD, Raman, SSTR). It was shown from HRXRD that the quality of the GaN layer improved with buffer layer thickness. AFM images did not show threading dislocations in the 10–15 μm-thick films (samples C and D). Raman spectroscopy analysis of the GaN E_2 (high) and A1 (LO) phonon modes confirmed lowest stress in these samples as well. Electrical characterization of fabricated

© 2023 Wiley-VCH GmbH

18626319, 2023, 16, Downloaded from https://onlinelibrary.wiley.com/doi/10.1002/pssa.202200828 by University Of Virginia Claude Moore, Wiley Online Library on [10/02/2024]. See the Terms and Conditions (https://onlinelibrary.wiley.com/terms-and-conditions) on Wiley Online Library for rules of use; OA articles are governed by the applicable Creative Commons License

AlGaN/GaN HEMTs showed somewhat higher off-state drain current ($I_{DS,OFF}$) in samples C and D, compared to sample B which had a 5 μm-thick buffer layer. The pulsed *I–V* measurements on the other hand showed that sample C had the most stable $R_{ON,DYN}$. Thermal resistance measurements on fabricated HEMTs agreed with the effective thermal conductivity k_{eff} obtained from the as-grown epilayers. This study suggests that the engineered substrate concept can support lateral AlGaN/GaN power device technology with a high-quality GaN buffer thickness of at least 10 μm, low leakage current and current collapse, and superior thermal performance owing to the high thermal conductivity of the GaN epitaxial layers and the AlN engineered substrate core.

Acknowledgements

Research at the Naval Research Laboratory was supported by the Office of Naval Research. Research at the Fraunhofer Institute for Applied Solid State Physics (IAF) was partially supported by the Office of Naval Research Global (Dr. Chip Eddy). J.S.L. gratefully acknowledges postdoctoral funding from the National Research Council.

Conflict of Interest

The authors declare no conflict of interest.

Data Availability Statement

The data that support the findings of this study are available from the corresponding author upon reasonable request.

Keywords

engineered substrate, gallium nitride, high electron mobility transistor, Raman spectroscopy, thermoreflectance

Received: November 28, 2022
Revised: April 13, 2023
Published online: June 1, 2023

[1] A. Krost, A. Dadgar, *Phys. State Solid A* **2002**, *194*, 361.
[2] F. J. Kub, K. D. Hobart, U.S. Patent No. 6,328,796, **2001**.
[3] F. J. Kub, K. D. Hobart, U.S. Patent No. 6,497,763, **2002**.
[4] K. D. Hobart, T. J. Anderson, A. D. Koehler, A. Nath, J. K. Hite, N. A. Mahadik, F. J. Kub, O. Aktas, V. Odnoblyudov, C. Basceri, in *CS Mantech Conf. Digest*, CS Mantech, Indian Wells, CA, May **2017**, p. 16.3.
[5] T. J. Anderson, A. D. Koehler, M. J. Tadjer, J. K. Hite, A. Nath, N. A. Mahadik, O. Aktas, V. Odnoblyudov, C. Basceri, K. D. Hobart, *Appl. Phys. Express* **2017**, *10*, 126501.
[6] T. J. Anderson, L. E. Luna, O. Aktas, G. M. Foster, A. D. Koehler, M. J. Tadjer, M. A. Mastro, K. D. Hobart, V. Odnoblyudov, C. Basceri, *ECS J. Solid State Sci. Technol.* **2019**, *8*, Q226.
[7] X. Li, K. Geens, W. Guo, S. You, M. Zhao, D. Fahle, V. Odnoblyudov, G. Groeseneken, S. Decoutere, *IEEE Electron Device Lett.* **2019**, *40*, 1499.
[8] K. Geens, X. Li, M. Zhao, W. Guo, D. Wellekens, N. Posthuma, D. Fahle, O. Aktas, V. Odnoblyudov, S. Decoutere, in *2019 IEEE 7th Workshop on Wide Bandgap Power Devices and Applications (WiPDA)*, Raleigh, NC, October **2019**, pp. 292–296. https://doi.org/10.1109/WiPDA46397.2019.8998922.
[9] X. Li, K. Geens, D. Wellekens, M. Zhao, A. Magnani, N. Amirifar, B. Bakeroot, et al., *IEEE Trans. Semicond. Manuf.* **2020**, *33*, 534.
[10] A. Zubair, J. Perozek, J. Niroula, O. Aktas, V. Odnoblyudov, T. Palacios, in *2020 Device Research Conf. (DRC)*, Columbus, OH, June **2020** https://doi.org/10.1109/DRC50226.2020.9135176.
[11] J. L. Braun, D. H. Olson, J. T. Gaskins, P. E. Hopkins, *Rev. Sci. Instrum.* **2019**, *90*, 024905.
[12] M. G. Burzo, P. L. Komarov, P. E. Raad, *IEEE Trans. Compon. Packag. Tech.* **2005**, *28*, 637.
[13] P. E. Raad, P. L. Komarov, M. G. Burzo, *Microelectr. J.* **2008**, *39*, 1008.
[14] W. Wang, L. Li, L. He, F. Yang, Z. Chen, Y. Zheng, L. He, Z. Wu, B. Zhang, Y. Liu, in *2016 13th China Int. Forum on Solid State Lighting: Int. Forum on Wide Bandgap Semiconductors China (SSLChina: IFWS)*, Beijing, China, November **2016**, pp. 77-80. https://doi.org/10.1109/IFWS.2016.7803761.
[15] M. Seon, T. Prokofyeva, M. Holtz, S. A. Nikishin, N. N. Faleev, H. Temkin, *Appl. Phys. Lett.* **2000**, *76*, 1842.
[16] T. Beechem, S. Graham, S. P. Kearney, L. M. Phinney, J. R. Serrano, *Rev. Sci. Instrum.* **2007**, *78*, 061301.
[17] M. Kuball, *Surf. Interface Anal.* **2001**, *31*, 987.
[18] J. S. Lundh, K. Coleman, Y. Song, B. A. Griffin, G. Esteves, E. A. Douglas, A. Edstrand, S. C. Badescu, E. A. Moore, J. H. Leach, B. Moody, S. Trolier-McKinstry, S. Choi, *J. Appl. Phys.* **2021**, *130*, 044501.
[19] S. Choi, E. Heller, D. Dorsey, R. Vetury, S. Graham, *J. Appl. Phys.* **2013**, *113*, 093510.
[20] A. F. Wilson, A. Wakejima, T. Egawa, *Appl. Phys. Express* **2013**, *6*, 086504.
[21] Y. Cao, J. W. Pomeroy, M. J. Uren, F. Yang, M. Kuball, *Nat. Electron.* **2021**, *4*, 478.
[22] J. Kuzmik, R. Javorka, A. Alam, M. Marso, M. Heuken, P. Kordos, *IEEE Trans. Electron Dev.* **2002**, *49*, 1496.
[23] D. Jin, J. A. del Alamo, *IEEE Trans. Electr. Dev.* **2013**, *60*, 3190.
[24] S. Martin-Horcajo, A. Wang, M.-F. Romero, M. J. Tadjer, F. Calle, *IEEE Trans. Electron Dev.* **2013**, *60*, 4105.
[25] M. J. Tadjer, T. J. Anderson, M. G. Ancona, P. E. Raad, P. Komarov, T. Bai, J. C. Gallagher, et al., *IEEE Electron Dev. Lett.* **2019**, *40*, 881.

© 2023 Wiley-VCH GmbH

18626319, 2023, 16, Downloaded from https://onlinelibrary.wiley.com/doi/10.1002/pssa.202200828 by University Of Virginia Claude Moore, Wiley Online Library on [10/02/2024]. See the Terms and Conditions (https://onlinelibrary.wiley.com/terms-and-conditions) on Wiley Online Library for rules of use; OA articles are governed by the applicable Creative Commons License